

Photon and Z Induced Heavy Charged Lepton Pair Production at a Hadron Supercollider

G. Bhattacharya, Pat Kalyniak and K. A. Peterson

Ottawa-Carleton Institute for Physics

Department of Physics, Carleton University

1125 Colonel By Drive, Ottawa, Ontario, Canada K1S 5B6

Abstract

We investigate the pair production of charged heavy leptons via photon-induced processes at the proposed CERN Large Hadron Collider (LHC). Using effective photon and Z approximations, rates are given for L^+L^- production due to $\gamma\gamma$ fusion and $Z\gamma$ fusion for the cases of inelastic, elastic and semi-elastic pp collisions. These are compared with the corresponding rates for production via the gluon fusion and Drell-Yan mechanisms. Various $\gamma\gamma$ and $Z\gamma$ differential luminosities for pp collisions are also presented.

PACS number(s): 13.85.-t, 14.60.Jj, 14.80.Am

I. INTRODUCTION

There has been a recent revival of interest in processes mediated via photons at e^+e^- colliders [1]. In the present work we address the question of photon induced production processes at hadron colliders, which have been relatively neglected. Since photons have a universal coupling to charged fermions it seems natural to consider fermion pair production as a benchmark process.

Heavy charged leptons are a feature of many models which extend the particle content of the Standard Model (SM). These include models which propose a complete additional generation [2] of heavy quarks and leptons, as well as those like E_6 based superstring-inspired models [3], which contain extra particles within each generation. The Drell-Yan [4], gluon fusion [5], and weak gauge boson fusion [6] mechanisms for the production of heavy charged leptons in hadron collisions have been investigated in the past. We here consider heavy charged lepton pair production in hadronic collisions via two photon ($\gamma\gamma$) and $Z\gamma$ fusion. In Fig. 1, we show the Feynman diagrams for the relevant subprocesses. We assume standard model couplings for both the γ and the Z boson to the heavy leptons, L .

The inelastic process $pp \rightarrow \gamma\gamma X \rightarrow L^+L^-X$ (where the photons come from the quarks), the elastic process $pp \rightarrow \gamma\gamma pp \rightarrow L^+L^-pp$ (where the photons come from the protons), and the semi-elastic process $pp \rightarrow \gamma\gamma pX \rightarrow L^+L^-pX$, are considered in a Weizsäcker-Williams approximation [7,8] (WWA). We have previously presented some results for these photon fusion processes [9], as have some other authors [10]. The inelastic $\gamma\gamma$ process was considered on its own by Eboli *et al.* [11] also.

Here, we also present heavy charged lepton pair production via $Z\gamma$ fusion. In fact, the $Z\gamma$ fusion process yields a larger production cross section than the $\gamma\gamma$ fusion over most of the lepton mass range we consider (m_L of 100 - 700 GeV). Our $Z\gamma$ fusion calculation is done within the framework of an effective vector boson approximation [12,13], for both inelastic and semi-elastic pp collisions. Heavy charged lepton production via $Z\gamma$ fusion has been previously considered for the case of inelastic pp collisions by Eboli *et al.* [11] We do

not agree with their results and discuss the origin of that discrepancy.

The organization of this paper is as follows. We describe in Sec. 2 the details of the effective photon and effective Z approximations which we have used. The $V\gamma$ ($V = \gamma, Z$) luminosities in pp collisions are presented in Sec. 3; these results are of broader interest than just for the particular heavy lepton production considered here. The L^+L^- production cross sections are presented in Sec. 4 and we summarize in the final section.

II. EFFECTIVE PHOTON AND EFFECTIVE Z APPROXIMATIONS

The central idea of the effective photon or Weizsäcker-Williams approximation [7] is to approximate the scattering cross-section involving a charged particle by a convolution of the equivalent number of photons in that particle with the relevant photoproduction cross-section. The quark-parton model has been very successful in describing hadronic interactions at high energies. For inelastic pp scattering a proton may be regarded essentially as a collection of freely travelling elementary constituent quarks and gluons. The Weizsäcker-Williams photon spectrum, $f_{\gamma/q}(x)$, from a quark (of charge e_q) is given by [14]

$$f_{\gamma/q}(x) = \frac{e_q^2}{8\pi^2} \frac{1 + (1-x)^2}{x} \log \frac{t_{\max}}{t_{\min}}. \quad (1)$$

where x is the fraction of the quark energy carried off by the photon. Here t_{\max} and t_{\min} are the characteristic maximum and minimum photon momentum transfers. For the process under consideration, pair production of heavy charged leptons of mass m_L , we have taken these to be $t_{\max} = \hat{s}/4 - m_L^2$, and $t_{\min} = 1 \text{ GeV}^2$, with \hat{s} being the center of mass energy in the parton frame. There is some flexibility in the choice of t_{\max} . However, in agreement with Altarelli *et. al.* [15], we have found that our results are not very sensitive to this parameter, within the limits of the Weizsäcker-Williams approximation. The particular choice of the minimum momentum transfer, t_{\min} , guarantees that the photons are obtained from the deep inelastic scattering of protons, when the quark-parton model is valid.

For inelastic scattering the incident proton ceases to exist and the constituents hadronize. However for elastic pp scattering the incident protons remain intact. The photon spec-

trum from protons for the elastic case, $f_{\gamma/p}^{\text{el}}$, has been derived by Kniehl [8] in a modified Weizsäcker-Williams approximation. It takes the form given below.

$$f_{\gamma/p}^{\text{el}}(x) = -\frac{\alpha}{2\pi}x \int_{-\infty}^{t_{\text{max}}} \frac{dt}{t} \left\{ 2 \left[\frac{1}{x} \left(\frac{1}{x} - 1 \right) + \frac{m_p^2}{t} \right] H_1(t) + H_2(t) \right\} \quad (2)$$

Here, $t_{\text{max}} = -m_p^2 x^2 / (1 - x)$ while H_1 and H_2 are functions of the electric and magnetic form factors of the proton of mass m_p , as given below.

$$H_1(t) = \frac{G_E^2(t) - (t/4m_p^2)G_M^2(t)}{1 - t/4m_p^2}, \quad H_2(t) = G_M^2(t) \quad (3)$$

The form factors are parametrized as

$$G_E(t) = (1 - t/0.71 \text{ GeV}^2)^{-2}, \quad G_M(t) = 2.79G_E(t). \quad (4)$$

Using these parametrizations Kniehl has obtained a closed analytic expression [8] for $f_{\gamma/p}^{\text{el}}$, which we have used in our calculation.

For hadron interactions at very high energies in the multi-TeV range, one can consider the W and Z bosons also as constituents of protons. In analogy with the effective photon approximation, effective vector boson approximations have been developed which considerably simplify calculations involving gauge bosons. However unlike photons, a massive gauge boson has both transverse and longitudinal polarizations and these degrees of freedom must be treated separately. The effective W and Z approximations give the spectra of longitudinally and transversely polarized W 's and Z 's from quarks in the protons.

We have done our calculations using two different forms for the effective Z approximation, the non-leading order Z distributions of Dawson [13] and those of Johnson *et. al.* [16]. In the original formulation of the approximation, Dawson [13] presents the distribution function of Z bosons in quarks both in the leading logarithmic (LL) approximation and also gives non-leading order corrections up to $\mathcal{O}(M_Z^2/E_q^2)$, where E_q is the quark energy. We used the non-leading order distribution in our calculation. An improved formulation of the effective vector boson approximation has been presented by Johnson *et. al.* [16]. This formulation does not invoke any kinematic approximations made in the original formulation, and claims

to improve the accuracy and extend the range of applicability of the effective vector boson approximation [16,17]. Dawson presents the distribution of transverse Z bosons averaged over the two transverse polarizations whereas Johnson *et. al.* derive separately each of the positive and negative helicity polarizations. The distribution expressions are too lengthy to reproduce here [13,16,17].

Johnson *et. al.*, in comparing their vector boson distribution functions with that of the leading logarithmic (LL) distribution functions of Dawson, find the LL expressions to be a considerable overestimate, particularly for small x and for the transverse polarization. We here find rather good agreement between our $Z\gamma$ luminosity results using the distribution functions of Dawson including non-leading order corrections and those of Johnson *et. al.*, as we show in the next Section.

III. PHOTON-PHOTON AND Z-PHOTON LUMINOSITIES

Using the effective photon and Z approximations described above we present here the two photon and Z -photon differential luminosities in pp collisions as a function of τ (the ratio of the $\gamma\gamma/Z\gamma$ subprocess energy and the total pp energy), for the inelastic, elastic and semi-elastic cases. These results are useful for adaptation to the production of other particles than heavy leptons.

The $V\gamma$ ($V = \gamma, Z$) differential luminosity for inelastic pp collisions is given by,

$$\frac{dL^{\text{inel}}}{d\tau}\Big|_{V\gamma/pp} = \sum_{i,j} \int_{\tau}^1 \frac{d\tau'}{\tau'} \int_{\tau'}^1 \frac{dx}{x} f_{q_i/p}(x) f_{q_j/p}(\tau'/x) \frac{dL}{d\xi}\Big|_{V\gamma/q_i q_j} \quad (5)$$

where $\xi = \tau/\tau'$ and

$$\frac{dL}{d\xi}\Big|_{V\gamma/q_i q_j} = \int_{\xi}^1 \frac{dx}{x} f_{V/q_i}(x) f_{\gamma/q_j}(\xi/x) \quad (6)$$

In the above expression $f_{q/p}$ represents the quark structure functions of the proton, which we have chosen to be the HMRS (Set B) structure functions [18]. For the case $V = \gamma$ an analytic expression can be obtained for the subprocess differential luminosity as

$$\frac{dL}{d\xi}\Big|_{\gamma\gamma/q_i q_j} = \frac{e_{q_i}^2 e_{q_j}^2}{64\pi^4} \left\{ \left(4 - \frac{6}{\xi} + 2\xi\right) - \left(4 + \frac{4}{\xi} + \xi\right) \log \xi \right\} \left(\log \frac{t_{\max}}{t_{\min}}\right)^2 \quad (7)$$

No such simple analytic expression is available for the case $V = Z$ using non-leading order Z distribution functions.

The $\gamma\gamma$ differential luminosity for elastic pp collisions is given by,

$$\frac{dL^{\text{el}}}{d\tau}\Big|_{\gamma\gamma/pp} = \int_{\tau/x_{\max}}^{x_{\max}} \frac{dx}{x} f_{\gamma/p}^{\text{el}}(x) f_{\gamma/p}^{\text{el}}(\tau/x) \quad (8)$$

where the upper limit of integration is given by kinematical considerations to be $x_{\max} = (1 - 2m_p/\sqrt{s})$, \sqrt{s} being the center of mass energy of the elastically colliding protons.

The $V\gamma$ ($V = \gamma, Z$) differential luminosity for semi-elastic pp collisions is given by,

$$\frac{dL^{\text{semi-el}}}{d\tau}\Big|_{V\gamma/pp} = 2 \int_{\tau/x_{\max}}^{x_{\max}} \frac{dx}{x} f_{\gamma/p}^{\text{el}}(x) f_{V/p}^{\text{inel}}(\tau/x) \quad (9)$$

where

$$f_{V/p}^{\text{inel}}(x) = \sum_i \int_{x_{\min}}^1 \frac{dx'}{x'} f_{q_i/p}(x') f_{V/q_i}(x/x') \quad (10)$$

We present $\gamma\gamma$ luminosities in Fig. 2, $Z\gamma$ luminosities derived with the non-leading Dawson effective Z approximation in Fig. 3, and $Z\gamma$ luminosities derived with the Johnson *et. al.* effective Z distributions in Fig. 4. We consider these results in turn below. The luminosity for the elastic case is independent of the production process, however for the other two cases it depends on the production process through the factor t_{\max} . In each Figure, the luminosities for inelastic and semi-elastic cases are presented for the case of charged lepton mass $m_L = 200$ GeV.

In Fig. 2 we show the inelastic, elastic, and semi-elastic two photon luminosities in pp collisions for the proposed CERN Large Hadron Collider (LHC) of center of mass energy of 14 TeV. For comparison purposes we also show the two gluon luminosity. As can be seen from Fig. 2 the $\gamma\gamma$ luminosities are comparable for the three cases but are, however, 3-4 orders of magnitude smaller than the gg luminosity. This can be understood as being due to the fact that the photon luminosities are suppressed by a factor $(\alpha/\alpha_s)^2$ with respect to

the gluon luminosity, which is somewhat countered by the logarithmic enhancement factor present in the photon luminosities.

In Figs. 3 a, b we show the $Z\gamma$ differential luminosities for inelastic and semi-elastic pp collisions, respectively, using the non-leading Dawson form of the effective Z approximation. The solid line corresponds to the luminosity for longitudinally polarized Z bosons, the dot-dashed line to the average over the two transverse polarizations of the Z . The luminosity corresponding to transversely polarized Z dominates that for longitudinal Z polarizations. This may be understood as being due to helicity suppression. For both the inelastic and semi-elastic cases, the $Z_T\gamma$ differential luminosity is larger than the $Z_L\gamma$ differential luminosity by a factor of 2-3 for $\tau \approx 10^{-3}$ and by an order of magnitude for $\tau \approx 10^{-1}$. Ultimately, however, we will see that the $Z_L\gamma \rightarrow L^+L^-$ cross-section dominates so it is most important to consider the luminosity for longitudinal Z bosons here. Comparing the inelastic and semi-elastic cases, the total differential $Z\gamma$ luminosity for the inelastic case is larger than that for the semi-elastic case by a factor of 2-3 for $\tau \approx 10^{-3}$, but for $\tau \geq 0.03$ they become equal.

In Figs. 4 a, b we show the results for the $Z\gamma$ differential luminosities, for inelastic and semi-elastic pp collisions, respectively, using the Johnson form of the effective Z approximation. Here, again, the solid line shows the luminosity for longitudinally polarized Z bosons. The dot-dashed and dotted lines show separately the luminosities for positive and negative helicity transverse Z polarizations, respectively. The dashed line corresponds to the sum of the luminosities for the two transverse Z polarizations, which we will refer to as Z_T as in the Dawson case. One observes essentially the same numerical relationships between the different luminosities shown here, as discussed above for the Dawson form of the effective Z approximation. The $Z_L\gamma$ luminosities agree almost exactly for the two different forms of the effective Z approximation, except at very small τ . The Johnson distribution functions yield $Z_T\gamma$ luminosities slightly larger than those obtained with the Dawson distribution functions. We will find that the $Z\gamma$ process cross section is only large enough to be interesting for heavy lepton masses above about 600 GeV; in the range of τ corresponding

to production of such heavy leptons the Dawson and Johnson luminosities for Z_T agree to 20 % or better. In both the longitudinal and transverse cases, one does expect some disagreement between the Dawson and Johnson formulations. While they are both non-leading distribution functions, they are derived under quite different kinematical assumptions; the Dawson derivation includes approximations, such as the small-angle one, which the Johnson derivation does not. In addition, for the transverse Z polarizations, the Johnson formulation separately extracts the positive and negative Z helicity distribution functions whereas the Dawson formulation extracts a single transverse Z distribution function from the cross sections averaged over the two transverse polarizations. So, particularly in the transverse case, the agreement should not be perfect. We have shown in Figs. 3 and 4 a detailed comparison of the luminosities using the two forms of the effective Z approximation. We will present the production cross-sections for $Z\gamma$ fusion using only the non-leading order Dawson form of the effective Z approximation in the next Section. This choice is really rather arbitrary. For the longitudinal Z case, which will be of interest, agreement between the two formulations is excellent.

Comparing the two different initiating states, we find that the $Z\gamma$ luminosities are smaller than the $\gamma\gamma$ luminosities for small values of τ , but they do not differ by more than an order of magnitude. For $\tau \geq 10^{-2}$ the $Z\gamma$ and $\gamma\gamma$ luminosities are of the same order of magnitude.

IV. THE L^+L^- PRODUCTION CROSS SECTIONS

The matrix elements and cross-sections for the relevant subprocesses, $V\gamma \rightarrow L^+L^-$, are given in the Appendix. The total cross-sections are obtained by convoluting the subprocess cross sections with the appropriate photon (and/or Z) and quark structure functions and integrating over the two body phase space using Monte Carlo techniques.

The cross-section for the $V\gamma$ production of a pair of heavy charged leptons in inelastic pp collisions (with center of mass energy \sqrt{s}) is obtained by convoluting the cross-section of the $V\gamma \rightarrow L^+L^-$ subprocess, $\sigma_{V\gamma}$, with the probabilities of finding the gauge bosons in the

protons as follows.

$$\sigma^{\text{inel}}(s) = \int_{x_{\text{min}}}^1 dx_1 \int_{x_{\text{min}}/x_1}^1 dx_2 f_{V/p}^{\text{inel}}(x_1) f_{\gamma/p}^{\text{inel}}(x_2) \sigma_{V\gamma}(x_1 x_2 s) \quad (11)$$

Here V represents either a photon or a longitudinal or transverse degree of freedom of the Z boson. The inelastic component of the V spectrum from protons, $f_{V/p}^{\text{inel}}(x)$, is given by

$$f_{V/p}^{\text{inel}}(x) = \int_{x_{\text{min}}}^1 dx_1 \int_{x_{\text{min}}/x_1}^1 dx_2 \sum_q f_{V/q}(x_1) f_{q/p}(x_2, Q^2) \delta(x - x_1 x_2) \quad (12)$$

In the above equation, the $f_{q/p}(x_2, Q^2)$ represent the quark structure functions for the proton [18], evaluated at the scale $Q^2 = \hat{s}/4$, \hat{s} being the parton center of mass energy squared. We sum over the contributions due to the u, d, c , and s quarks and antiquarks from the protons. The lower limit of integration in the above equations ensures that the $V\gamma$ center of mass energy is sufficient for L^+L^- production.

The cross-section for two photon L^+L^- production via elastic collisions of protons is obtained by folding the $\gamma\gamma$ subprocess cross-section, $\sigma_{\gamma\gamma}$, with the elastic component of the photon spectrum from the protons, $f_{\gamma/p}^{\text{el}}$.

$$\sigma^{\text{el}}(s) = \int_{x_{\text{min}}}^{x_{\text{max}}} dx_1 \int_{x_{\text{min}}/x_1}^{x_{\text{max}}} dx_2 f_{\gamma/p}^{\text{el}}(x_1) f_{\gamma/p}^{\text{el}}(x_2) \sigma_{\gamma\gamma}(x_1 x_2 s) \quad (13)$$

The upper limits of integration in the above expression are given by $x_{\text{max}} = 1 - 2m_p/\sqrt{s}$, where \sqrt{s} is the center of mass energy of the elastically colliding protons. The lower limit of integration x_{min} has the same significance as in the case of inelastic collisions. We have checked this calculation by using an alternative form of the photon spectrum from elastically colliding protons [19]. The cross sections obtained with this alternative form essentially agree with the results presented here using the Kniehl form of WWA.

The cross sections for L^+L^- production via semi-elastic collisions of protons, induced by $\gamma\gamma$ and $Z\gamma$ are obtained in a similar fashion by appropriately combining the two cases detailed above.

For comparison with the mechanisms considered here, we also present results for the two previously well known production mechanisms for L^+L^- , Drell-Yan and gluon fusion. The

Drell-Yan quark anti-quark annihilation proceeds via s-channel γ and Z exchange. The gluon fusion proceeds via a quark triangle diagram followed by Z boson or Higgs boson exchange. Expressions for these cross sections can be found in the literature [5,20]. The rates for the other possible processes of weak gauge boson fusion and annihilation are negligible compared to the Drell-Yan and gluon fusion rates except for the case of very massive heavy leptons, [5] and will not be discussed further.

In our calculations we use $M_W = 80.22$ GeV, $M_Z = 91.19$ GeV. In calculating the two photon production cross-sections we have taken into account the variation of the fine structure constant α with the energy scale, e.g., we have chosen $\alpha = 1/137$ in the expressions for Weizsäcker-Williams photon spectrum, and $\alpha = 1/128$ in the expressions for the subprocess cross-sections. The parameter α_s , used in the gluon fusion calculation, is evaluated at the two-loop level using its representation in the modified minimal-subtraction ($\overline{\text{MS}}$) scheme [21], and using the value $\Lambda_{\overline{\text{MS}}}^{(4)} = 0.19$ GeV, consistent with the HMRS (Set B) parametrization. For the gluon fusion mechanism we assume three generations of quarks, with the top quark mass set at 175 GeV. Results for the inclusion of a fourth generation of heavy quarks can be found in Refs. 2, 19. The Higgs boson mass for our calculation is chosen to be 200 GeV. There is very little sensitivity to this parameter.

The total cross sections for L^+L^- production via two photon fusion as a function of the charged lepton mass, are shown in Fig. 5 for the LHC center of mass energy of 14 TeV. The dotted and upper solid curves represent respectively the cross sections due to gluon fusion and Drell-Yan mechanisms. The lower solid curve represents the total cross section for the inelastic process $pp \rightarrow \gamma\gamma X \rightarrow L^+L^- X$. The dashed and dot-dashed curves show the corresponding cross-sections for the elastic and semi-elastic cases respectively. The cross-sections for the three cases are comparable to each other over the mass range of the charged lepton. However they are 2-3 orders of magnitude smaller than the Drell-Yan and gluon fusion cross sections.

Hence in general, production rates via two photon fusion at pp colliders are not competitive with production via quark or gluon fusion. Only the interesting event topology of

particle production through photon fusion for elastic and semi-elastic pp collisions might offer a chance of distinguishing signals which are otherwise very difficult in a hadronically noisier environment. Both the elastic and semi-elastic processes should yield clean events with the intact proton(s) continuing in the forward direction. However, the low event rates probably eliminate this as a viable process for L^+L^- discovery. Two recent publications [10] address similar topics for two photon processes as discussed here, and reach essentially the same conclusions. Drees *et al.* point out the additional problem of multiple events at high luminosity; thus, the high luminosity necessary to achieve an interesting rate will destroy the cleanliness of the signal.

We now turn to the L^+L^- production via $Z\gamma$ fusion. In the Appendix, we present the matrix element squared for the $Z\gamma$ subprocess, without summing over the Z boson polarization. This allows us to obtain separately the contributions from longitudinally and transversely polarized Z bosons. We also give an expression for the subprocess cross-section summed over Z boson polarizations in the Appendix.

For subprocess energies much greater than the Z boson mass the interactions between the longitudinally polarized Z boson and fermions can be derived in terms of an effective theory [22] in which z_L is the would be Goldstone boson of the broken $SU(2)_L \times U(1)_Y$ model. Calculations are greatly simplified in the effective theory since the vector bosons are replaced by scalar bosons. Hence as an additional check on our exact calculation we have calculated the cross-section for the subprocess $Z_L\gamma \rightarrow L^+L^-$ in the Goldstone boson approximation. The subprocess cross-section for longitudinal Z bosons dominates since the coupling of fermions to longitudinally polarized Z bosons is proportional to the large fermion mass in the effective Lagrangian, as given by Dawson [6]

$$\mathcal{L} \sim \frac{ig}{2M_Z \cos \theta_W} m_L \bar{l} \gamma_5 l z_L \quad (14)$$

Here l indicates the heavy charged lepton wave function and z_L that of the Goldstone boson. The subprocess cross-section is given in the Appendix. Indeed we find good agreement between this approximate calculation and our results obtained from the exact calculation.

In Figs. 6 a, b we show respectively the L^+L^- production cross-sections via $Z\gamma$ fusion at the LHC for inelastic and semi-elastic pp collisions. We have used the non-leading Dawson form of the Z distribution function. For reference, the cross sections due to gluon fusion and Drell-Yan mechanisms are again shown as the dotted and upper solid curves, respectively. The dashed and dot-dashed curves represent, respectively, the separate contributions of longitudinally and transversely polarized Z bosons. The solid curve is the total cross section. The $Z_T\gamma$ cross-section is smaller than that for $Z_L\gamma$ and also decreases more rapidly with increasing m_L . For small values of m_L the cross-sections for semi-elastic pp collisions are smaller than those for inelastic collisions, but they become approximately equal for $m_L \geq 500$ GeV.

Our results for $Z\gamma$ production of heavy charged lepton are in disagreement with those of Eboli *et al.* [11] Those authors consider inelastic $Z\gamma$ production in pp collisions using the leading logarithmic result for the effective Z approximation, and using the Goldstone boson approximation for the subprocess cross-section. However, as has been pointed out in Ref. 6, they have chosen the Z_L coupling to quarks in the effective Lagrangian to be proportional to the vector coupling of Z bosons to quarks, whereas it should be proportional to the axial vector coupling. They find the transversely polarized Z boson cross-sections dominating the longitudinally polarized Z boson cross-section. While we agree that the $Z_T\gamma$ luminosity is larger than that for $Z_L\gamma$, we find that the $Z_L\gamma \rightarrow L^+L^-$ cross-section dominates. As noted above we have good agreement between our exact calculation and the Goldstone boson approximation calculation for the $Z_L\gamma$ subprocess.

One can see that the $Z\gamma$ inelastic cross-sections are comparable to the $\gamma\gamma$ inelastic cross-sections for small values of m_L . However the $\gamma\gamma$ fusion cross-section falls off much more rapidly with increasing m_L compared to the $Z\gamma$ fusion cross-section, and for larger values of m_L the $Z\gamma$ cross-section is an order of magnitude larger than the $\gamma\gamma$ cross-section. One may intuitively understand the relative magnitudes of the $\gamma\gamma$ and $Z\gamma$ cross-sections as follows. The ratio of the subprocess cross-sections for $Z\gamma \rightarrow L^+L^-$ and $\gamma\gamma \rightarrow L^+L^-$ for the same subprocess center of mass energy (i.e. same τ) is almost independent of τ but depends

only on m_L . The $Z\gamma$ subprocess cross-section is approximately an order of magnitude larger than that for $\gamma\gamma$ for $m_L \approx 200$ GeV and is about two orders of magnitude larger for $m_L \approx 700$ GeV. Since the $Z\gamma$ differential luminosities in pp collisions are about an order of magnitude smaller than the $\gamma\gamma$ differential luminosities for small τ , and approximately equal for $\tau \geq 10^{-2}$, the relative magnitudes of the total cross-sections obtained in pp collisions follow.

The result is that each of the inelastic and semi-elastic $Z\gamma$ production cross sections for L^+L^- is within about an order of magnitude of the Drell-Yan and gluon fusion cross sections for large values of m_L , beyond m_L about 500 GeV in the inelastic case and somewhat higher in the semi-elastic case. For these large lepton masses, the cross sections for the $Z\gamma$ processes are down at the tenths of a fb level, so high luminosity is again important. A one year integrated luminosity of 100 fb^{-1} provides about 20 pairs of 600 GeV leptons for each of the inelastic and semi-elastic mechanisms.

We now discuss qualitatively the possible signatures for L^+L^- pair production at pp colliders via $Z\gamma$ fusion and their potential backgrounds. We have discussed the production of L^+L^- so far in a relatively model-independent fashion. The production cross-sections for heavy charged leptons that are predicted within a large variety of models, are either given directly by the cross-section results presented here or can be obtained by a simple rescaling of these results. The decays for heavy charged leptons and their possible signatures depend however on other extra particles predicted within the model. Thus a model independent discussion of the observability of L^+L^- pairs is not possible. Previous work on detailed analysis of L^+L^- signal and backgrounds by Barger *et. al.* [2] and I. Hinchliffe [24] assumed a sequential (4th generation) charged heavy lepton and its associated neutrino ν_L . For simplicity we consider the same model here in our discussion of the possible signatures. Depending on the decay mode of charged heavy leptons there can be three possible signatures which we discuss in turn.

If both charged heavy leptons decay leptonically, *e.g.* $L^+ \rightarrow \bar{\nu}_L \bar{l} \nu_l$, $L^- \rightarrow \nu_L l' \bar{\nu}_{l'}$ ($l, l' = e, \mu$), the signature would be an e^+e^- , or $\mu^+\mu^-$, or $e^\pm\mu^\mp$ pair and missing transverse

momentum. The SM backgrounds in this case are: (a) $pp \rightarrow Z^*\gamma^* \rightarrow \tau\bar{\tau}$ (b) $pp \rightarrow W^+W^-$ (c) $pp \rightarrow ZZ$ (d) $pp \rightarrow t\bar{t} \rightarrow bW^+\bar{b}W^-$ where the gauge bosons and τ leptons themselves decay leptonically. There are also additional backgrounds to be considered, the two-photon fusion processes at pp colliders, $\gamma\gamma \rightarrow W^+W^-$ and $\gamma\gamma \rightarrow l\bar{l}$. If one heavy lepton decays leptonically and the other hadronically, *e.g.* $L^+ \rightarrow \bar{\nu}_L q\bar{q}'$, $L^- \rightarrow \nu_L l\bar{\nu}_l$, the final state consists of an electron or muon, missing p_T and jets. The SM backgrounds for this signature are : (a) $pp \rightarrow W^- + \text{jets}$ (b) $pp \rightarrow W^+W^-$ (c) $pp \rightarrow t\bar{t} \rightarrow bW^+\bar{b}W^-$, and the process $\gamma\gamma \rightarrow W^+W^-$, where for the cases of W pair production, one W boson of the pair decays leptonically and the other hadronically. If both charged heavy leptons decay hadronically the signature is 4 jets and missing p_T . The SM background in this case is $pp \rightarrow Z + 4 \text{ jets}$, with $Z \rightarrow \nu\bar{\nu}$.

Detailed Monte-Carlo simulations of the signals and backgrounds for these decay modes of L , but corresponding to a different production mode, in inelastic pp collisions, have been reported previously [2,24]. For the semi-elastic $Z\gamma$ fusion case, the signals corresponding to the various decay modes of L considered above would include the additional tag of a single proton. In principle the unique topology of the semi-elastic $Z\gamma$ events could be exploited to observe the signal, for example by using forward spectrometers. The results presented here are intended as an exploratory survey of the novel signatures that occur in photon and Z induced fusion processes at hadron colliders. Detailed confirmation of the observability of these signatures would require Monte-Carlo simulations of the signals and backgrounds, including considering the detector acceptance, and effects such as overlapping events at high luminosities.

V. CONCLUSIONS

We have evaluated the importance of hadron colliders as a source of $\gamma\gamma$ and $Z\gamma$ collisions by considering the production of charged heavy leptons in such colliders. While we have used the pair production of charged heavy leptons as a benchmark process, some of our results are of broader interest. In particular, we have presented $\gamma\gamma$ and $Z\gamma$ luminosities for inelastic,

elastic, and semi-elastic pp scattering. The luminosities for longitudinally and transversely polarized Z bosons were given separately. These results can be used for the consideration of the production of other final states via the $\gamma\gamma$ and $Z\gamma$ initiating subprocesses.

Our conclusions with respect to the two photon induced heavy lepton production are rather pessimistic, consistent with Drees *et al.* [10]. The total event rates for $\gamma\gamma$ induced processes are not competitive with other dominant production mechanisms, being down by a couple orders of magnitude. The novel mechanism of obtaining photons without one or both of the protons breaking up could, in principle, prove useful in confirming signals which are difficult to otherwise distinguish. However, the $\gamma\gamma$ cross sections are probably too suppressed to exploit the topology of the elastic events.

On the other hand, we find that $Z\gamma$ production of heavy charged leptons overtakes $\gamma\gamma$ production for lepton masses above 100 GeV. It rises to within about an order of magnitude of the dominating Drell-Yan and gluon fusion processes for m_L of about 600 GeV. This is the same sort of behaviour as seen in Higgs boson production via the gluon and vector boson fusion mechanisms, where the vector boson fusion cross-section ultimately overtakes the gluon fusion cross-section for large Higgs mass [23]. Hence the $Z\gamma$ initiated processes should not be neglected. The inelastic and semi-elastic processes together make up about 10% of the total event rate for m_L of 600 GeV. The cleaner semi-elastic production could in principle stand out as a distinguishable signal, however direct confirmation of that requires detailed detector simulation studies.

ACKNOWLEDGMENTS

This work was funded in part by the Natural Sciences and Engineering Research Council of Canada. The authors acknowledge useful conversations with Rohini Godbole, Manuel Drees and Dieter Zeppenfeld.

APPENDIX:

We present here expressions for the squared matrix elements and subprocess cross-sections for L^+L^- pair production through $\gamma\gamma$ and $Z\gamma$ fusion.

Assuming that heavy charged leptons couple to the photon in the usual way, the summed and averaged matrix element squared for the 2 photon fusion subprocess is given by

$$\begin{aligned} \sum \overline{|\mathcal{M}_{\gamma\gamma}|^2} = 2e^4 \left[\frac{(u - m_L^2)}{(t - m_L^2)} + \frac{(t - m_L^2)}{(u - m_L^2)} - 4m_L^2 \left(\frac{1}{(t - m_L^2)} + \frac{1}{(u - m_L^2)} \right) \right. \\ \left. - 4m_L^4 \left(\frac{1}{(t - m_L^2)} + \frac{1}{(u - m_L^2)} \right)^2 \right] \end{aligned} \quad (\text{A1})$$

where t and u refer to the exchanged momenta squared corresponding to the direct and crossed diagrams (Figs. 1 a, b) for the two photon subprocess, and the photon coupling is represented by $e^2 = 4\pi\alpha$, with the value of the fine structure constant $\alpha = 1/128$ which is appropriate for high energy production processes. The total subprocess cross-section for $\gamma\gamma \rightarrow L^+L^-$ is given by

$$\sigma(\gamma\gamma \rightarrow L^+L^-) = \frac{e^4}{4\pi s^2} \left[\left(\frac{8m_L^4}{s} - 4m_L^2 - s \right) \log \left(\frac{1 - \beta}{1 + \beta} \right) - \beta(s + 4m_L^2) \right] \quad (\text{A2})$$

where $\beta = (1 - 4m_L^2/s)^{\frac{1}{2}}$, s being the $\gamma\gamma$ center of mass energy.

We present the matrix element squared for the $Z\gamma$ subprocess after summing and averaging over the photon polarization but not the Z polarization.

$$\sum_{\gamma} \overline{|\mathcal{M}_{Z\gamma}|^2} = \frac{e^4}{x_W(1 - x_W)} \left[\frac{T_1}{(t - m_L^2)^2} + \frac{T_2}{(u - m_L^2)^2} + \frac{T_3}{(t - m_L^2)(u - m_L^2)} \right] \quad (\text{A3})$$

where

$$\begin{aligned} T_1 = 2 \left[(g_V^2 + g_A^2) \left\{ (t - u)m_L^2 + ut - 4Q'^2(t - 3m_L^2) - 4QQ'(t - m_L^2) - 2M_Z^2m_L^2 + 3m_L^4 \right\} \right. \\ \left. - 2(g_V^2 - g_A^2) \left\{ m_L^2(t + m_L^2) \right\} \right] \end{aligned} \quad (\text{A4})$$

$$T_2 = T_1(Q \leftrightarrow Q', t \leftrightarrow u) \quad (\text{A5})$$

$$\begin{aligned} T_3 = 4 \left[(g_V^2 + g_A^2) \left\{ (t + u)(m_L^2 - M_Z^2) + 2Q^2(t + m_L^2 - M_Z^2) + 2Q'^2(u + m_L^2 - M_Z^2) \right. \right. \\ \left. \left. + 2QQ'(t + u - 2m_L^2) - 2m_L^2M_Z^2 + 2m_L^4 + M_Z^4 \right\} \right. \\ \left. - (g_V^2 - g_A^2) \left\{ m_L^2(4Q^2 + 4Q'^2 + 8QQ' + t + u - 2M_Z^2) + 2m_L^4 \right\} \right] \end{aligned} \quad (\text{A6})$$

In the above expressions $g_V = (-\frac{1}{4} + x_W)$ and $g_A = \frac{1}{4}$ are respectively the vector and axial vector couplings of the heavy lepton to Z boson, $x_W = \sin^2 \theta_W$, θ_W being the Weinberg angle, and

$$Q = q \cdot \epsilon_Z, \quad Q' = q' \cdot \epsilon_Z \quad (\text{A7})$$

where ϵ_Z is the Z polarization vector and q, q' are, respectively the L^- and L^+ momentum 4-vectors.

Summing and averaging over Z polarizations, the total subprocess cross-section for $Z\gamma \rightarrow L^+L^-$ is given by

$$\begin{aligned} \sigma(Z\gamma \rightarrow L^+L^-) = & \frac{e^4}{6x_W(1-x_W)} \frac{8}{16\pi(s-M_Z^2)^2} \left[(g_V^2 - g_A^2) \left\{ -\frac{12s\beta m_L^2}{s-M_Z^2} + \frac{m_L^2}{s-M_Z^2} (2M_Z^2 \right. \right. \\ & - 16s + 24m_L^2 + 2\frac{s^2}{M_Z^2}) \log\left(\frac{1-\beta}{1+\beta}\right) \left. \right\} + (g_V^2 + g_A^2) \left\{ -2\beta(s-M_Z^2) \right. \\ & + 4s\beta \frac{m_L^2 - M_Z^2}{s-M_Z^2} + \log\left(\frac{1-\beta}{1+\beta}\right) (-2(s-m_L^2 - M_Z^2) \\ & \left. \left. + \frac{m_L^2}{s-M_Z^2} \left(6s + 8M_Z^2 - 8m_L^2 - \frac{4sM_Z^2}{m_L^2} - 2\frac{s^2}{M_Z^2} \right) \right) \right] \end{aligned} \quad (\text{A8})$$

where $\beta = (1 - 4m_L^2/s)^{\frac{1}{2}}$, s being the $Z\gamma$ center of mass energy.

The expression for the total cross-section for the subprocess $Z_L\gamma \rightarrow L^+L^-$, in the Goldstone boson approximation, is given by:

$$\begin{aligned} \sigma(Z_L\gamma \rightarrow L^+L^-) = & \frac{e^4}{3x_W(1-x_W)} \frac{m_L^2}{16\pi M_Z^2 (s-M_Z^2)^2} \left\{ M_Z^2 \left(\frac{-2s\beta}{s-M_Z^2} \right) \right. \\ & \left. - 2\log\left(\frac{1-\beta}{1+\beta}\right) \left[\frac{1}{2}(s-M_Z^2) + M_Z^2 \left(\frac{s-2m_L^2}{s-M_Z^2} \right) \right] \right\} \end{aligned} \quad (\text{A9})$$

REFERENCES

- [1] For a review see *e.g.* *Proceedings of the Conference on Physics and Experiments at Linear Colliders*, Saariselkä, Finland, edited by R. Orava, Eerola and Nordberg, (World Scientific 1992); *Proceedings of the IX th International Workshop on Photon-Photon Collisions*, La Jolla, California, edited by D.O. Caldwell and H.P. Paar, World Scientific (1992); *Proceedings of the Workshop on Physics and Experiments with Linear e^+e^- Colliders*, Waikoloa, Hawaii, edited by F. A. Harris, S. L. Olsen, S. Pakvasa and X. Tata, World Scientific (1993).
- [2] V. Barger, T. Han and J. Ohnemus, *Phys. Rev.* **D37**, 1174 (1988) and references therein.
- [3] J.L. Hewett and T.G. Rizzo, *Phys. Rep.* **183**, 193 (1989).
- [4] S.D. Drell and T.M. Yan, *Phys. Rev. Lett.* **25**, 316 (1970); *Ann. Phys. (NY)* **66**, 578 (1971).
- [5] S.S.D. Willenbrock and D.A. Dicus, *Phys. Lett.* **B 156**, 429 (1985).
- [6] S. Dawson and S.S.D. Willenbrock, *Nucl. Phys.* **B 284**, 449 (1987).
- [7] E.J. Williams, *Proc. R. Soc. London (A)* **139**, 163 (1933); *Phys. Rev.* **45**, 729(L) (1934); C.F. von Weizsäcker, *Z. Phys.* **88**, 612 (1934).
- [8] B.A. Kniehl, *Phys. Lett.* **B 254**, 267 (1991).
- [9] G. Bhattacharya, P.A. Kalyniak and K.A. Peterson, *Proc. of the Workshop on Physics at Current Accelerators and Supercolliders*, Argonne, Illinois, edited by J.L. Hewett, A.R. White and D. Zeppenfeld, (1993)p531; G. Bhattacharya, P.A. Kalyniak, and K.A. Peterson, *Proceedings of the 16th Annual MRST (Montréal-Rochester-Syracuse-Toronto) Meeting on High Energy Physics: What Next? Exploring the Future of High Energy Physics*, Montréal, Canada, edited by J.F. Cudell, K.R. Dienes, and B. Margolis (1994) p261.

- [10] M. Drees, R.M. Godbole, M. Nowakowski and S.D. Rindani, Phys. Rev. **D50**, 2335 (1994); J. Ohnemus, T.F. Walsh and P.M. Zerwas, Phys. Lett. **B328**, 369 (1994)
- [11] O.J.P. Éboli, G.C. Marques, S.F. Novaes, and A.A. Natale, Phys. Rev. **D34**, 771 (1986)
- [12] G.L. Kane, W.W. Repko, and W.B. Rolnick, Phys. Lett. **B148**, 367 (1984); J. Lindfors, Z. Phys. **C28**, 427 (1985)
- [13] S. Dawson, Nucl. Phys. **B 249**, 42 (1985)
- [14] S.J. Brodsky, T. Kinoshita, and H. Terazawa, Phys. Rev. **D4**, 1532 (1971); H. Terazawa, Rev. Mod. Phys. **45**, 615 (1973)
- [15] G. Altarelli, G. Martinelli, B. Mele and R. Rückl, Nucl. Phys. **B262**, 204 (1985).
- [16] P.W. Johnson, F.I. Olness and W.K. Tung, Phys. Rev. **D36**, 291 (1987)
- [17] R.M. Godbole and F.I. Olness, Int. J. Mod. Phys. **A 2**, 1025, (1987)
- [18] P.N. Harriman, A.D. Martin, R.G. Roberts and W.J. Stirling, Phys. Rev. **D42**, 798 (1990).
- [19] K. Hagiwara, S. Komamiya and D. Zeppenfeld, Z. Phys. **C 29**, 115 (1985); M. Drees and D. Zeppenfeld, Phys. Rev. **D 39**, 2536 (1989).
- [20] R.M. Barnett *et al.*, *Proceedings of the Summer Study on High Energy Physics in the 1990s*, Snowmass, Colorado (World Scientific 1988)
- [21] W. Marciano, Phys. Rev. **D29**, 580 (1984).
- [22] M. Chanowitz, M. Furman and I. Hinchliffe, Phys. Lett. **B78**, 285 (1978); Nucl. Phys. **B153**, 402 (1979)
- [23] R.N. Cahn and S. Dawson, Phys. Lett. **B136**, 196 (1984); Erratum Phys. Lett. **B138**, 464 (1984).
- [24] I. Hinchliffe, Int. J. Mod. Phys. **A4**, 3867 (1989).

FIGURES

FIG. 1. The Feynman diagrams which contribute to the subprocess $V\gamma \rightarrow L^+L^-$ ($V = \gamma, Z$).

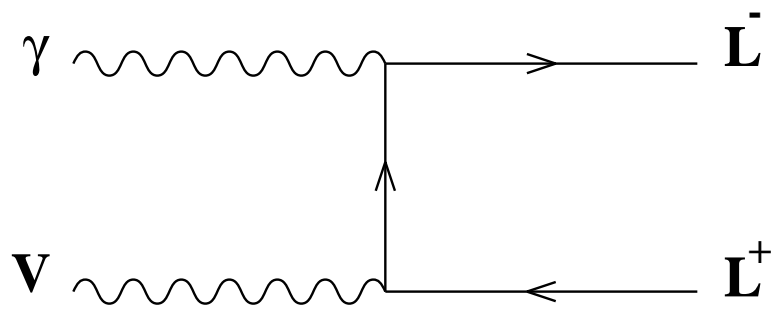
FIG. 2. The differential gg and $\gamma\gamma$ luminosities in pp collisions at the LHC ($\sqrt{s} = 14$ TeV). The solid, dashed and dot-dashed curves represent respectively the $\gamma\gamma$ luminosities for inelastic, elastic and semi-elastic pp collisions. The inelastic and semi-elastic luminosities are shown for the case when the charged leptons produced via photon fusion has mass $m_L = 200$ GeV. The dotted curve shows the gluon luminosity.

FIG. 3. The differential $Z\gamma$ luminosities in pp collisions at the LHC ($\sqrt{s} = 14$ TeV) corresponding to the non-leading Dawson form of the effective Z approximation. (a) The solid and dot-dashed curves represent, respectively, the $Z\gamma$ luminosities due to the longitudinal and transverse Z boson polarizations for inelastic pp collisions. (b) The curves have the same meaning as in (a) except that they are for semi-elastic pp collisions. The luminosities shown in both figures are for the case when the charged leptons produced via $Z\gamma$ fusion have mass $m_L = 200$ GeV.

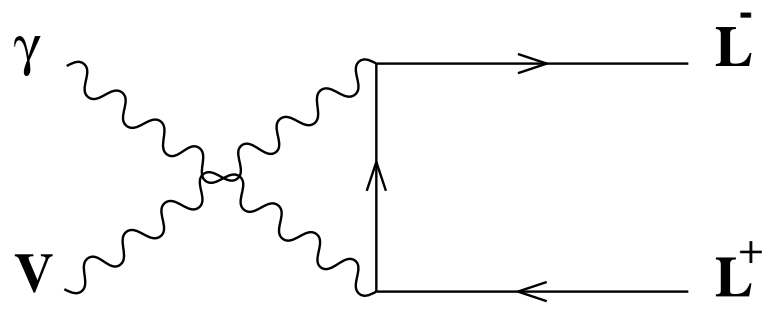
FIG. 4. The differential $Z\gamma$ luminosities in pp collisions at the LHC ($\sqrt{s} = 14$ TeV) corresponding to the Johnson form of the effective Z approximation. (a) The solid, dot-dashed and dotted curves represent respectively the $Z\gamma$ luminosities due to the longitudinal, positive helicity, and negative helicity transverse Z boson polarizations for inelastic pp collisions. The dashed curve represents the luminosity for the sum of the two transverse Z polarizations. (b) The curves have the the same meaning as in (a) except that they are for semi-elastic pp collisions. The luminosities shown in both figures are for the case when the charged leptons produced via $Z\gamma$ fusion have mass $m_L = 200$ GeV.

FIG. 5. The total production cross section (in femtobarns) for a heavy charged lepton pair in pp collisions at the LHC ($\sqrt{s} = 14$ TeV). The upper solid curve and the dotted curve show, respectively, the Drell-Yan and gluon fusion cross sections. The lower solid curve, dashed and dot-dashed curves represent respectively the photon fusion cross-sections for inelastic, elastic and semi-elastic pp collisions.

FIG. 6. The total production cross section (in femtobarns) for a heavy charged lepton pair in pp collisions at the LHC ($\sqrt{s} = 14$ TeV) using the non-leading Dawson distribution functions. In each of (a) and (b), the upper solid curve and the dotted curve show, respectively, the Drell-Yan and gluon fusion cross sections. (a) The dashed and dot-dashed curves represent, respectively, the longitudinal and transverse Z boson contributions to the $Z\gamma$ fusion cross-sections for inelastic pp collisions. The lower solid curve shows the total inelastic $Z\gamma$ fusion cross-section. (b) The curves have the same meaning as in (a) except that they are for semi-elastic pp collisions.



(a)



(b)

Fig. 1

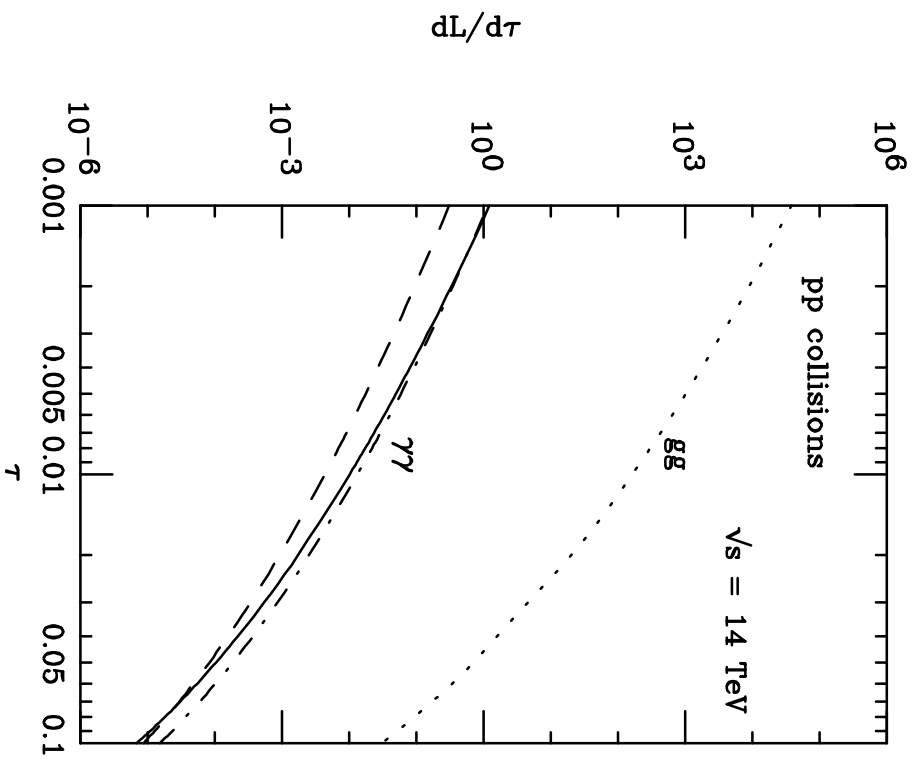


Fig. 2

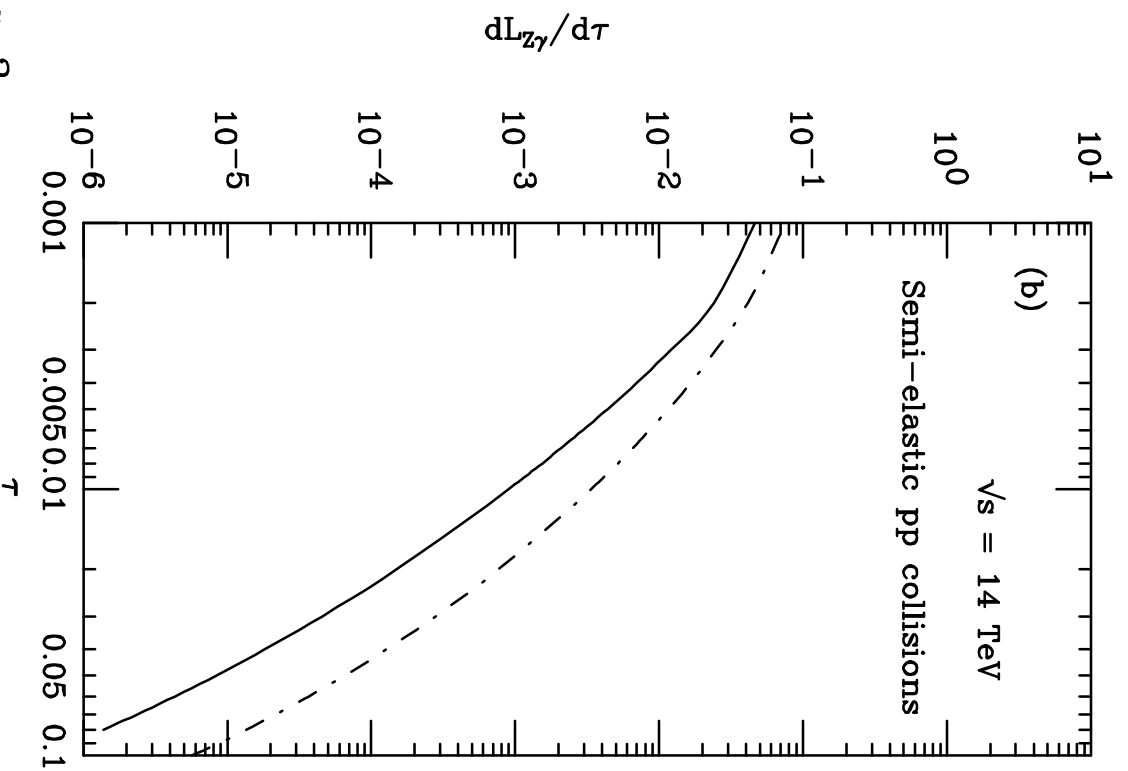
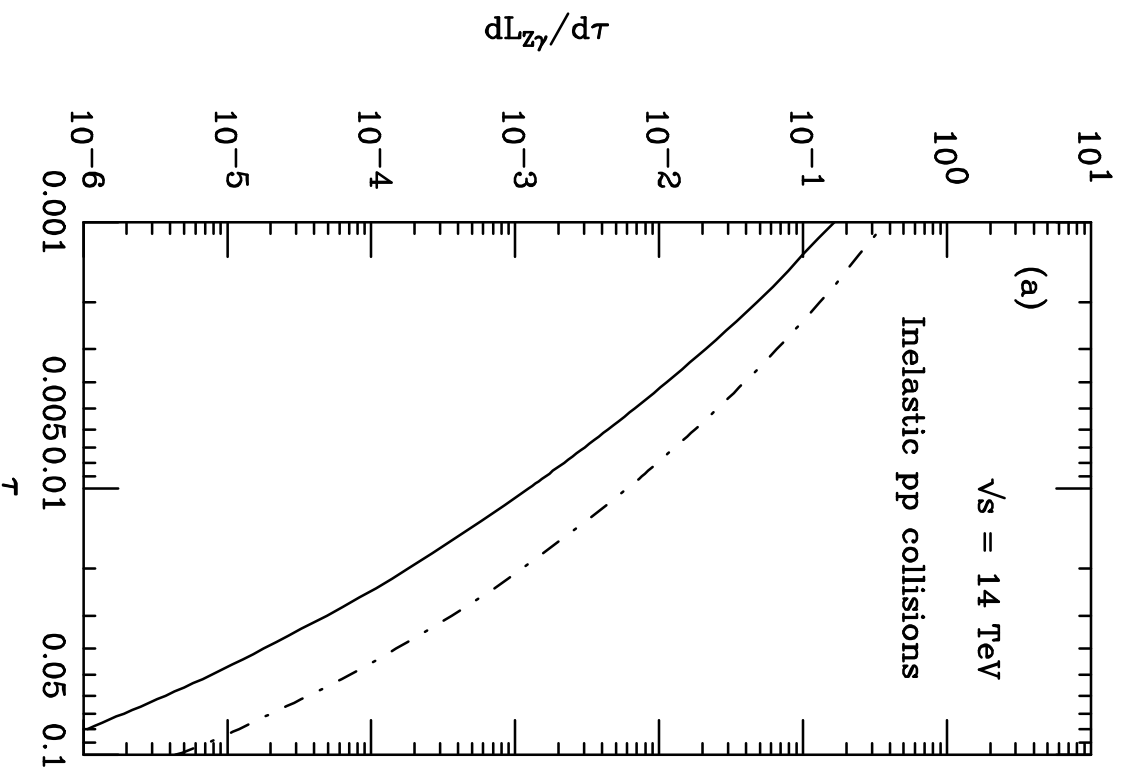


Fig. 3

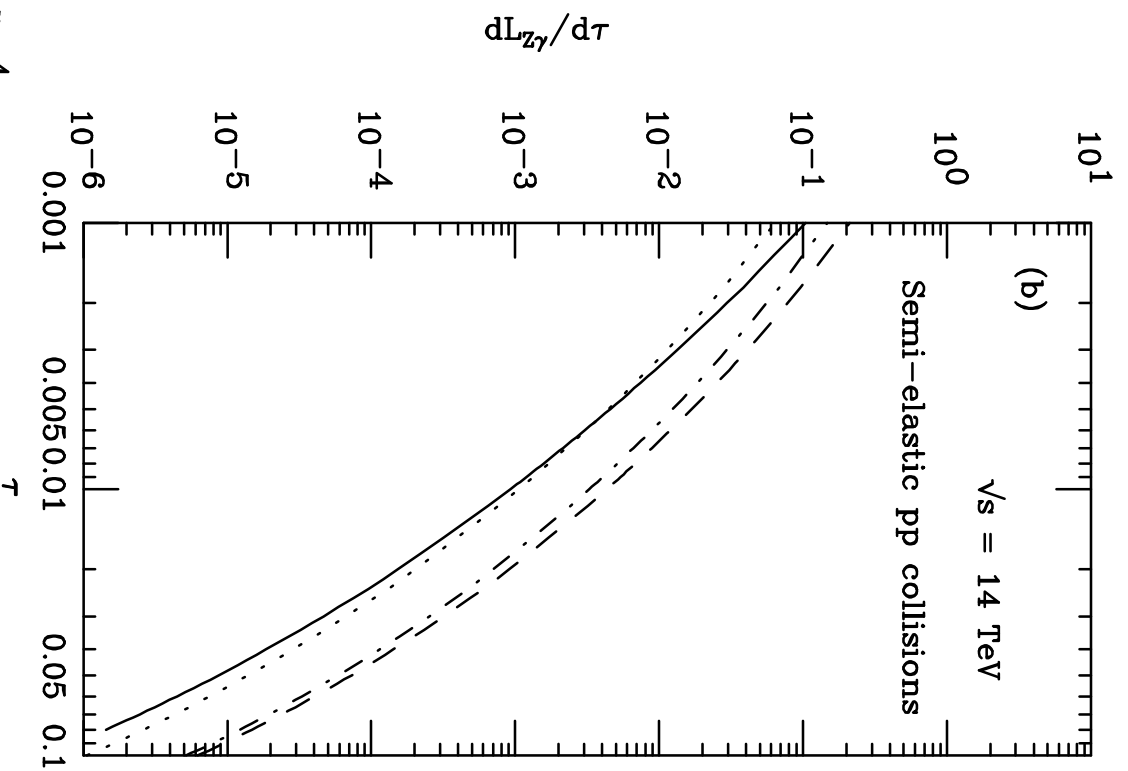
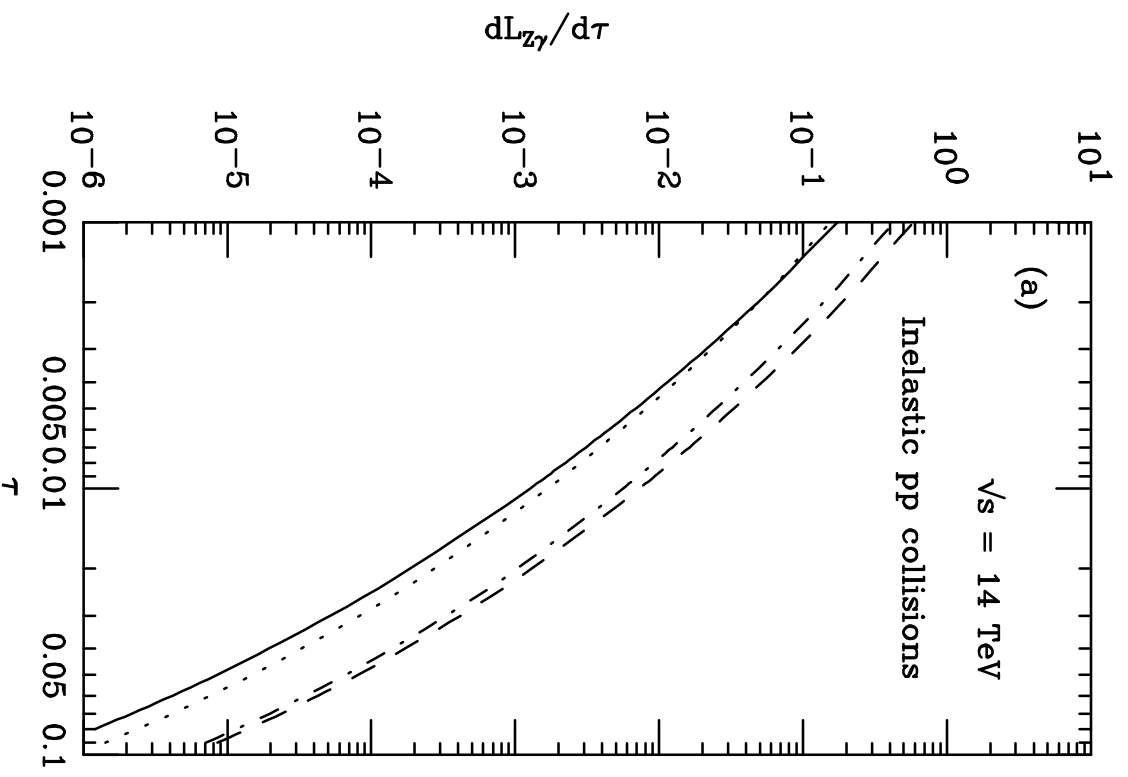


Fig. 4

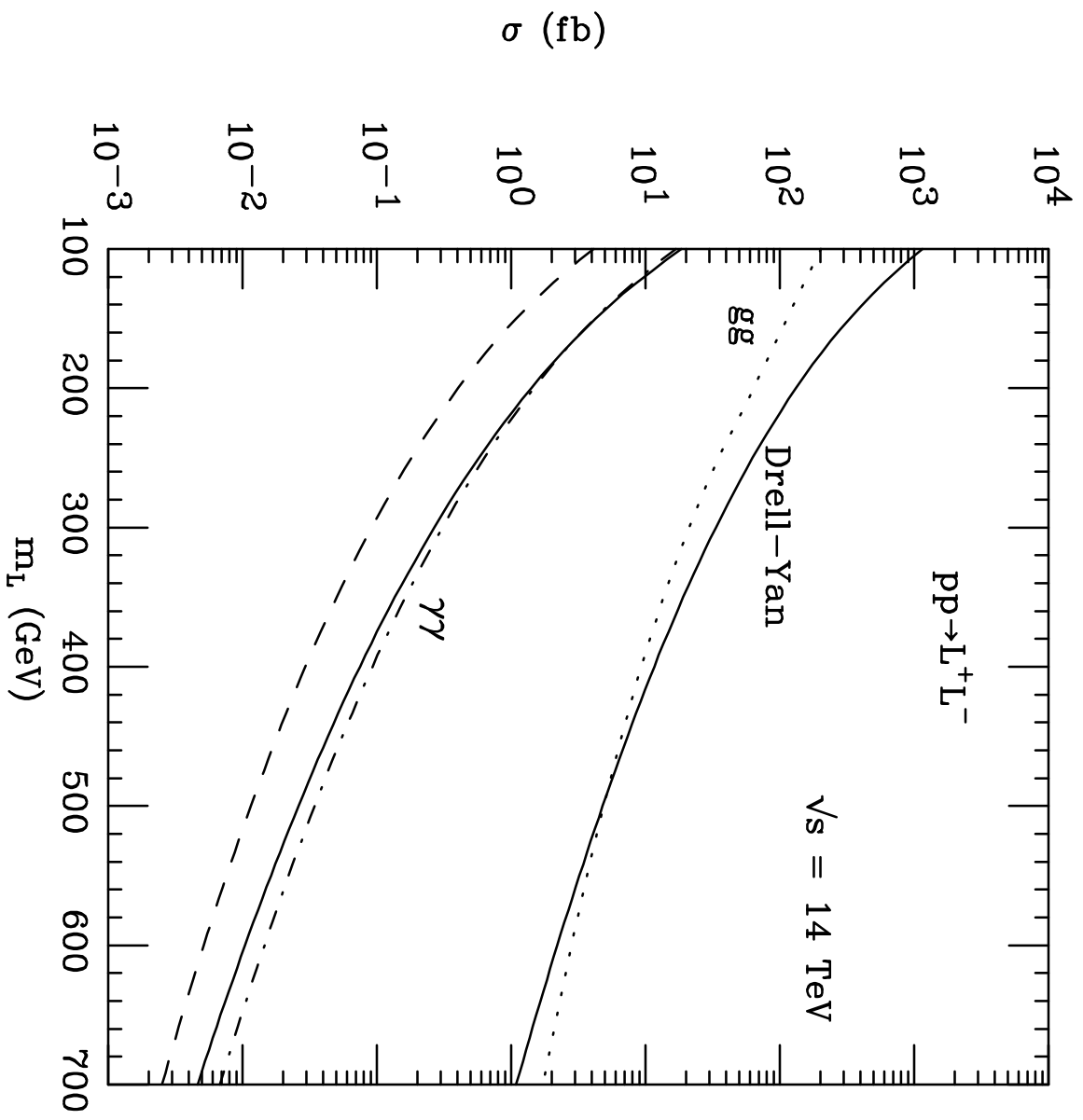


Fig. 5

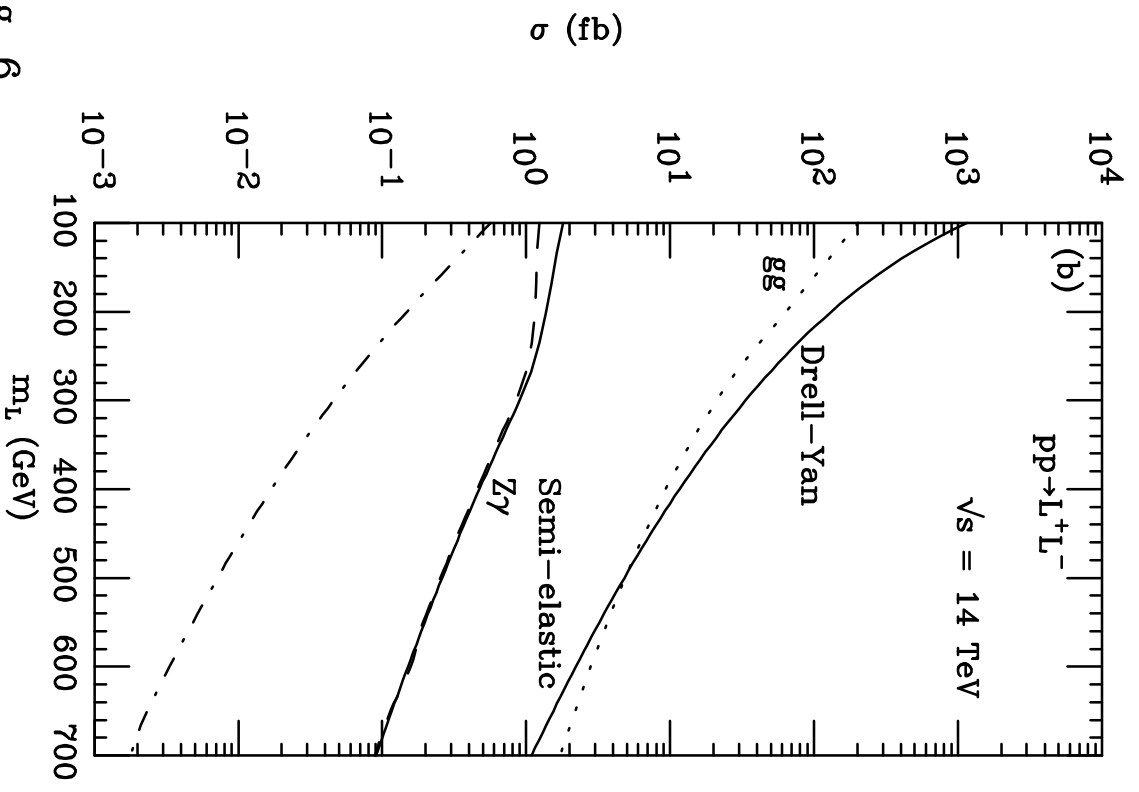
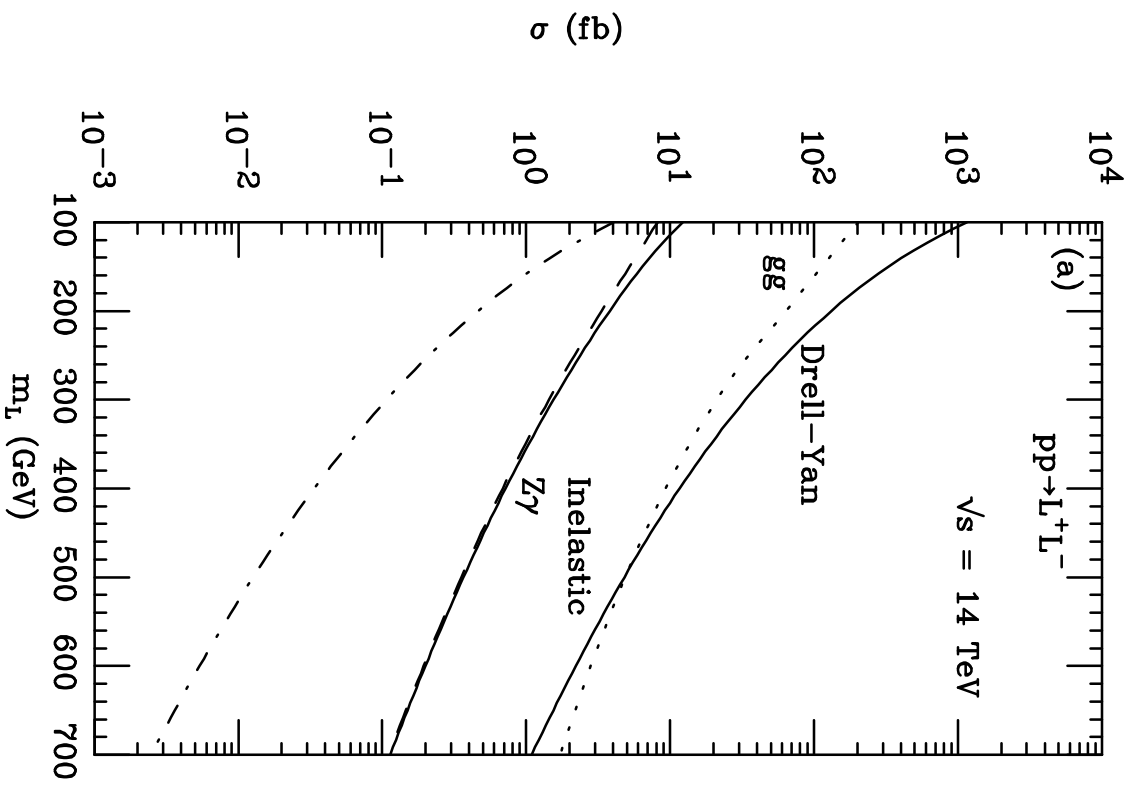


Fig. 6